

## Enhancement of Quasistationary Shocks and Heating via Temporal Staging in a Magnetized Laser-Plasma Jet

D. P. Higginson,<sup>1,2,\*</sup> B. Khair,<sup>3,4</sup> G. Revet,<sup>1,5</sup> J. Béard,<sup>6</sup> M. Blecher,<sup>7</sup> M. Borghesi,<sup>8</sup> K. Burdonov,<sup>5</sup> S. N. Chen,<sup>1,5</sup> E. Filippov,<sup>9,10</sup> D. Khaghani,<sup>11</sup> K. Naughton,<sup>8</sup> H. Pépin,<sup>12</sup> S. Pikuz,<sup>9,10</sup> O. Portugall,<sup>6</sup> C. Riconda,<sup>13</sup> R. Riquier,<sup>1,14</sup> R. Rodriguez,<sup>15</sup> S. N. Ryazantsev,<sup>9,16</sup> I. Yu. Skobelev,<sup>9,10</sup> A. Soloviev,<sup>5</sup> M. Starodubtsev,<sup>5</sup> T. Vinci,<sup>1</sup> O. Willi,<sup>7</sup> A. Ciardi,<sup>3,4</sup> and J. Fuchs<sup>1,5</sup>

<sup>1</sup>Laboratoire pour l'Utilisation des Lasers Intenses–CNRS, CEA, École Polytechnique, Univ. Paris-Saclay, Sorbonne Univ., UPMC Univ. Paris 06, F-91128 Palaiseau cedex, France

<sup>2</sup>Lawrence Livermore National Laboratory, Livermore, California 94551, USA

<sup>3</sup>Sorbonne Univ., UPMC Univ. Paris 6, UMR 8112, LERMA, F-75005 Paris, France

<sup>4</sup>LERMA, Observatoire de Paris, PSL Research University, CNRS, UMR 8112, F-75014 Paris, France

<sup>5</sup>Institute of Applied Physics, 46 Ulyanov Street, 603950 Nizhny Novgorod, Russia

<sup>6</sup>LNCMI, UPR 3228, CNRS-UGA-UPS-INSA, 31400 Toulouse, France

<sup>7</sup>Institut für Laser- und Plasmaphysik, Heinrich-Heine-Universität Düsseldorf, D-40225 Düsseldorf, Germany

<sup>8</sup>Centre for Plasma Physics, Queen's University Belfast, Belfast BT7 INN, United Kingdom

<sup>9</sup>Joint Institute for High Temperatures, RAS, 125412 Moscow, Russia

<sup>10</sup>National Research Nuclear University "MEPhI," 115409 Moscow, Russia

<sup>11</sup>GSI Helmholtzzentrum für Schwerionenforschung GmbH, 64291 Darmstadt, Germany

<sup>12</sup>INRS-ÉMT, 1650 bd. L. Boulet, J3X1S2 Varennes, Québec, Canada

<sup>13</sup>LULI, Sorbonne Univ.–UPMC Univ. Paris 06, École Polytechnique, CNRS, CEA, 75005 Paris, France

<sup>14</sup>CEA, DAM, DIF, 91297 Arpajon, France

<sup>15</sup>Departamento de Física de la Universidad de Las Palmas de Gran Canaria, E-35017 Las Palmas de Gran Canaria, Spain

<sup>16</sup>M.V. Lomonosov Moscow State University, 119991 Moscow, Russia

(Received 3 June 2017; revised manuscript received 25 October 2017; published 22 December 2017)

We investigate the formation of a laser-produced magnetized jet under conditions of a varying mass ejection rate and a varying divergence of the ejected plasma flow. This is done by irradiating a solid target placed in a 20 T magnetic field with, first, a collinear precursor laser pulse ( $10^{12}$  W/cm<sup>2</sup>) and, then, a main pulse ( $10^{13}$  W/cm<sup>2</sup>) arriving 9–19 ns later. Varying the time delay between the two pulses is found to control the divergence of the expanding plasma, which is shown to increase the strength of and heating in the conical shock that is responsible for jet collimation. These results show that plasma collimation due to shocks against a strong magnetic field can lead to stable, astrophysically relevant jets that are sustained over time scales 100 times the laser pulse duration (i.e., > 70 ns), even in the case of strong variability at the source.

DOI: 10.1103/PhysRevLett.119.255002

Whereas a large amount of work has been done concerning the vacuum expansion of a laser-produced plasma and its inertial collimation through, for example, different geometrical target configurations or particular focusing of the laser [1–4], experiments with external magnetic fields strong enough to affect the plasma dynamics or energy transport have been made possible only recently. Such studies are pertinent to concepts related to both laser-[5] and magnetically driven [6] inertial confinement fusion that combine high-power lasers with strong magnetic fields to increase implosion stability [7,8] and improve yields [9]. Related experiments have already shown significant modifications to energy transport [10,11] due to the magnetic field. However, little attention has been paid so far to the role of a strong externally applied magnetic field on the laser ablation dynamics or on the influence of time-variable ejections on the plasma evolution.

Within the context of high-energy density laboratory astrophysics, the coupling of laser-driven plasmas with an externally imposed magnetic field has proven successful in diverse areas, examples are the generation of collisionless shocks [12] and studies related to magnetized accretion columns [13] and magnetically collimated jets [14–17]. High-aspect-ratio, supersonic jets are ubiquitous in astrophysics (e.g., in young stellar objects [18] and active galactic nuclei [19]), and are the result of magnetic fields mediating the extraction of energy from an accreting system [20]. While not yet studied in the laboratory, variability of the mass ejection rate plays an important role in structuring astrophysical jets, for example, by generating velocity fluctuations large enough to produce internal shocks in the flow [21].

In this Letter we investigate the collimation, heating, long-range jet formation, and stability of plasma flows

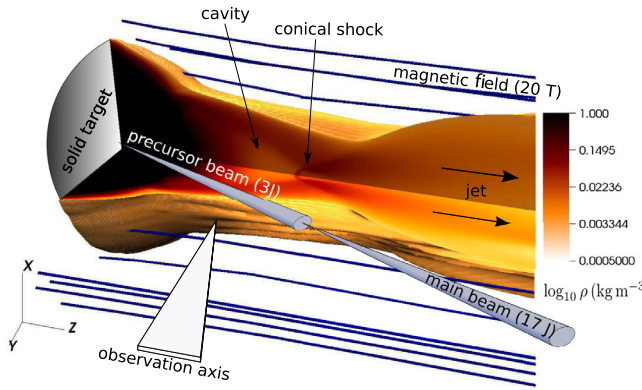


FIG. 1. Schematic of the experimental setup and 3D MHD simulations of the overall plasma dynamics. The volume rendering shows the simulated mass density at 22 ns, for the case of a single 17 J pulse, with 1/4 of the volume removed to show the internal flow structure. Two collinear laser pulses (3 and 17 J), that are temporally offset by either 9 or 19 ns, irradiate a  $(\text{C}_2\text{F}_4)_n$  target embedded in a 20 T magnetic field. The diagnostic observation axis is also shown.

ejected in a burstlike manner in a magnetized vacuum. We irradiate a solid Teflon [i.e.,  $(\text{C}_2\text{F}_4)_n$ ] target with one or two (temporally delayed) high-power laser pulses to generate a hot plasma expanding in a 20 T (axial) magnetized vacuum. The characteristic plasma conditions near the target and its interaction with the external magnetic field are substantially modified by the temporal modulation of the energy deposition. The delay between the precursor and main laser pulses controls the spatial extent over which most of the main laser energy is absorbed, with longer delays leading to more spherical plasma expansions, stronger shocks, and enhanced plasma heating. On the other hand, we observe that at distances far from the target, magnetically collimated, astrophysically relevant jets and recollimation conical shocks can be sustained for time scales over 100 times ( $> 70$  ns) the laser pulse duration, and show remarkable stability despite the strong variations at the ejecta source.

The experiment was performed using the chirped Nd: glass laser ( $\tau_L = 0.6$  ns,  $\lambda_L = 1057$  nm) of the ELFIE facility at the Laboratoire pour l'Utilisation des Lasers Intenses (LULI). The laser beam was split temporally into two beams, separated by either 9 or 19 ns, and subsequently recombined collinearly using nonpolarizing beam splitters and focused on target (diameter,  $\phi_L = 0.7$  mm) using the same lens and random phase plate [22]. In the temporally staged configuration, the first beam, called the precursor, had an on-target energy (intensity) of 3 J ( $1 \times 10^{12}$  W/cm<sup>2</sup>) and the second pulse, called the main pulse, had 17 J ( $7 \times 10^{12}$  W/cm<sup>2</sup>). Additionally, a main-pulse-only setup (i.e., identical but without the precursor) was used for comparison. As shown in Fig. 1, both beams irradiated a  $(\text{C}_2\text{F}_4)_n$  target immersed in a 1  $\mu\text{s}$  pulsed, 20 T external magnetic field aligned along the plasma expansion axis

[17,23]. The plasma electron density evolution was investigated via a Mach-Zehnder interferometer using a 5 ps ( $\lambda_L = 528$  nm) probe beam. Optical emission along the same line of sight was studied through a one-dimensional slice taken along the jet propagation axis and streaked in time using a Hamamatsu C7700 streak camera with S20 photocathode. To diagnose electron temperature  $T_e$ , a time-integrated x-ray focusing spectrometer with spatial resolution (FSSR) was used along the jet axis. The relative intensities of He-like fluorine lines were analyzed to obtain time-integrated  $T_e$  and electron density  $n_e$  [24,25]. Alongside the experiments, we performed simulations with the 3D Eulerian, radiative (optically thin approximation), resistive magnetohydrodynamic (MHD) code GORGON [26,27] with an initially uniform magnetic field in the  $z$  direction. The initial laser deposition (up to 1 ns) is modeled in axisymmetric, cylindrical geometry with the two-dimensional, three-temperature, radiative (diffusion approximation), Lagrangian, hydrodynamic code DUED [28], which is then passed to GORGON. The purpose of this hand-off is to take advantage of the capability of the Lagrangian code to achieve very high resolution in modeling the laser-target interaction. We note that for this laser energy and target material, radiation transport will not substantially influence the expansion of the laser plume. This method has been benchmarked against a variety of laser and target conditions such as those presented in Refs. [15,17]. To introduce the second pulse, we implemented a laser deposition module in GORGON that assumes linear inverse-bremsstrahlung absorption and the geometric optics approximation. We note that 3D modeling is important to capture azimuthal Rayleigh-Taylor-type instabilities developing at plasma-vacuum interface that can create a relatively low density, broad halo [14].

The top row of Fig. 2 shows plasma electron density  $n_e$  at three times in the main-pulse-only case. The plasma dynamics consist of three distinct phases (for an extensive discussion, see Refs. [14,15]): (i) creation of a low density cavity surrounded by a shock envelope [Fig. 2(a)], (ii) formation of a conical shock [Fig. 2(d)] at the tip of the cavity, which then (iii) recollimates the plasma plume into a jet [Fig. 2(g)]. These phases are also captured in the MHD simulations shown in Fig. 5. The next two rows in Fig. 2 show  $n_e$  maps in the two laser-pulse cases with either 9 or 19 ns delay between the precursor and main laser pulses.

Let us focus first on the cavity formation and the surrounding shock envelope [Figs. 2(a)–2(c), 5(b), and 5(c)]. Initially, the ram pressure of the plasma plume,  $P_{dy} = \rho v^2$ , is much larger than the magnetic pressure,  $P_m = B^2/2\mu_0$ , and the plasma expansion proceeds unimpeded ( $\rho$  is mass density,  $v$  is flow velocity,  $B$  is magnetic field strength). Our simulations indicate that 2 ns after the main pulse arrival, the dynamic plasma  $\beta$  ( $\beta_{dy} = P_{dy}/P_m$ ) is  $\sim 10^3$ . The expanding plasma plume has a relatively high magnetic Reynolds number ( $\text{Re}_m = vL/\eta \sim 100$ ); thus, the

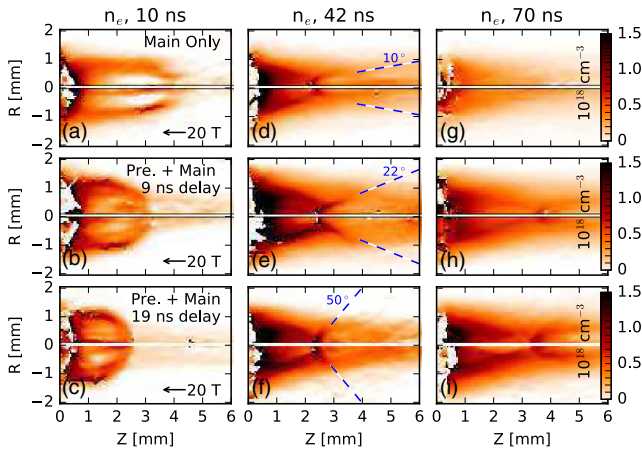


FIG. 2. Plasma electron density measured via interferometry, and analyzed using Abel inversion [29,30], in pseudocolor with identical color scales as shown on the right. The central pixels are removed due to the uncertainty of the Abel inversion on axis. Notice that the images appear very symmetric. The three columns show times of 10 (a–c), 42 (d–f), and 70 ns (g–i) measured from the beginning of the main pulse irradiation. The top row (a,d,g) shows the case of main pulse alone, the middle (b,e,h) and bottom (c,f,i) rows show the temporally staged cases of 9 and 19 ns delay, respectively.

magnetic field is “frozen” in the plasma as predicted by ideal MHD. For  $Re_m$  we use characteristic velocity  $v = 100$  km/s, length scale  $L = 1$  mm, and magnetic diffusivity  $\eta = 10^4$  cm<sup>2</sup>/s. Both thermal conduction and viscosity are unimportant in the formation of the cavity and jet, as exemplified by relatively large Peclet and Reynolds numbers,  $Pe \gtrsim 10$  and  $Re \gtrsim 10^4$  [14,15,17].

From x-ray spectrometry measurements in the cavity at  $z = 1$  mm, we infer  $T_e \sim 40$ –60 eV (Fig. 3). We quantify the relative importance of optically thin radiative cooling on the energy budget by estimating the characteristic cooling time scale, defined as the ratio of thermal energy density over radiated power density. For the characteristic temperatures and densities found in the flow, the cooling time scale is in the range  $\sim 10$ –100 ns. This indicates that cooling by radiation can be important in some localized regions, such as shocks.

The cavity is formed by the “frozen-in” magnetic field being advected by the plasma flow, leading to an increase of the magnetic pressure on the edges of the expanding plasma. The radial expansion is then halted when ram and magnetic pressures become comparable ( $\beta_{dy} \sim 1$ ). The slowing down of the plasma flow by the magnetic field leads to the formation of a reverse shock, observed as a jump in density around the edges of the cavity (see Fig. 2), and to plasma heating (see Fig. 3).

While the general flow structure is similar with and without precursor irradiation, it is clear that adding a precursor laser pulse crucially modifies the dynamics and physical characteristics of the plasma in the cavity. Electron density maps taken at the same time (10 ns) after

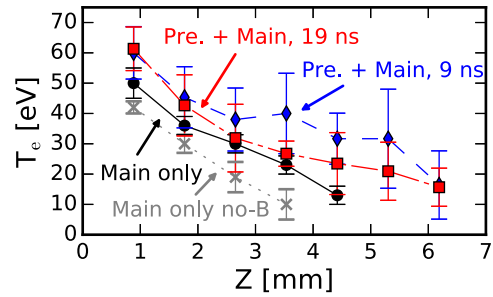


FIG. 3. X-ray spectrometry measurements of  $T_e$  from the FSSR. Lines with circles ( $\times$ 's) represent the main-pulse-only setup with (without) an applied 20 T  $B$  field. Lines with diamonds and squares show cases with a precursor of 9 and 19 ns delay, respectively.

the arrival of the main pulse [Figs. 2(a)–2(c)] show the cavity becoming more spherical when the precursor laser pulse is used. The relatively small, 14%, increase in the radial extent of the cavity is accompanied by a considerable reduction in its longitudinal extent: from 4 mm with the main pulse only to around 2.5 mm with the addition of the precursor offset by 19 ns. We notice that in the two-pulse configurations higher  $n_e$  is measured ( $2 \times 10^{19}$  cm<sup>−3</sup>) along the shocks bounding the cavity [see, in particular, Figs. 2(d)–2(f)], a clear sign that shocks are stronger. This agrees with the  $T_e$  measurements shown in Fig. 3, which are larger with temporally staging. Additionally, as shown in Fig. 4, optical emission inside the cavity ( $z < 2$  mm) is clearly enhanced, both in intensity and duration, when

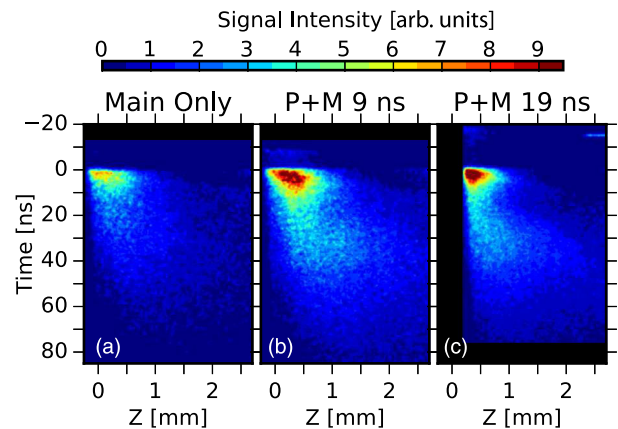


FIG. 4. Streaked optical emission profiles along the center of the plasma expansion axis (smoothed with a 5-pixel Gaussian) plotted with the same linear color scale for (a) the main-pulse-only case and (b) [(c)] the precursor and main pulses with a 9 ns [19 ns] delay between them. Time is measured from the beginning of the main pulse. Note the small signal from the precursor interaction in (b) [(c)] at  $-9$  ns [ $-19$  ns]. The profiles in (a) and (b) were taken over successive shots and with the exact same detector settings. Profile (c) was taken at a later time and thus was slightly scaled and shifted for comparison with the previous profiles. The thin streak in (c) at  $t = -15$  ns,  $z = 2.25$  mm is from the interferometry probe.

adding the precursor. Non-local thermodynamic equilibrium calculations of photon absorption in the visible range (400–550 nm) corresponding to the S20 cathode response for a  $\text{CF}_2$  plasma show that above  $T_e = 10$  eV and below  $n_e = 10^{19} \text{ cm}^{-3}$  the photon mean-free path is greater than 30 mm, indicating an optically thin regime in this range. Given the high  $T_e$  and given that optical emission decreases with temperature in this regime, the brighter areas seen in Fig. 4 indicate the presence of denser plasma, consistent with the interferometric data.

Differences in the plasma properties and flow dynamics when introducing the precursor pulse can be understood by considering the location in the precursor plasma where the energy of the main laser pulse is absorbed. Figure 5(a) shows the simulated density produced by the precursor pulse at the time of the arrival of the main pulse (considering 19 ns separation). The fast expansion of the plasma in the  $z$  direction (100–500 km/s) causes rapid changes in the longitudinal  $n_e$  profiles. These are shown in Fig. 5(d) at three different times for both the magnetized (solid lines) and an unmagnetized (dashed lines) case of precursor irradiation. In the figure, regions where  $n_e$  is in the range from 0.1 to 1.0  $n_c$ , where  $n_c = 10^{21} \text{ cm}^{-3}$  is the critical density of the laser, are highlighted with thicker lines; in this region over 90% of the laser energy from the main pulse is absorbed. From this plot it is clear that the  $n_e$  profiles for the unmagnetized and magnetized cases are essentially identical up to 50 ns with substantial differences arising only in the low density regions where laser absorption is insignificant. The applied 20 T magnetic field thus does not alter the absorption of the main laser pulse and only plays a role in the plasma dynamics following the laser absorption. Nonetheless, because of the expansion of the precursor plasma, the region over which most of the main laser is absorbed moves away from the initial target surface and increases in longitudinal extent  $L_{\text{abs}}$  as well as volume,  $V_{\text{abs}} \sim L_{\text{abs}} \phi_L^2$ . Thus, the absorbing plasma becomes more cylindrical and has lower thermal pressure ( $\sim E_L/V_{\text{abs}}$ ), when using two pulses and for longer time delays. The longitudinal stretching of  $L_{\text{abs}}$  causes more plasma to be accelerated radially and the overall expansion to be more divergent. This is consistent with the experiments, which show a more spherical expansion for the double pulse cases and for longer time delays [Figs. 2(b) and 2(c)]. Further corroboration comes from Fig. 5(e), which shows a reduction of the ratio of the longitudinal to radial kinetic energy in the main-pulse-only case compared to two pulses and for longer delays.

Collimation of the plasma plume into a jet takes place through a conical shock, which forms 2–4 mm from the initial target [Figs. 2(d)–2(i)]. The conical shock is the result of oblique shocks redirecting the plasma flow along the cavity walls and towards its tip [14]. In particular, we find that the opening angle of the conical shock and jet depends on the laser irradiation conditions, increasing from

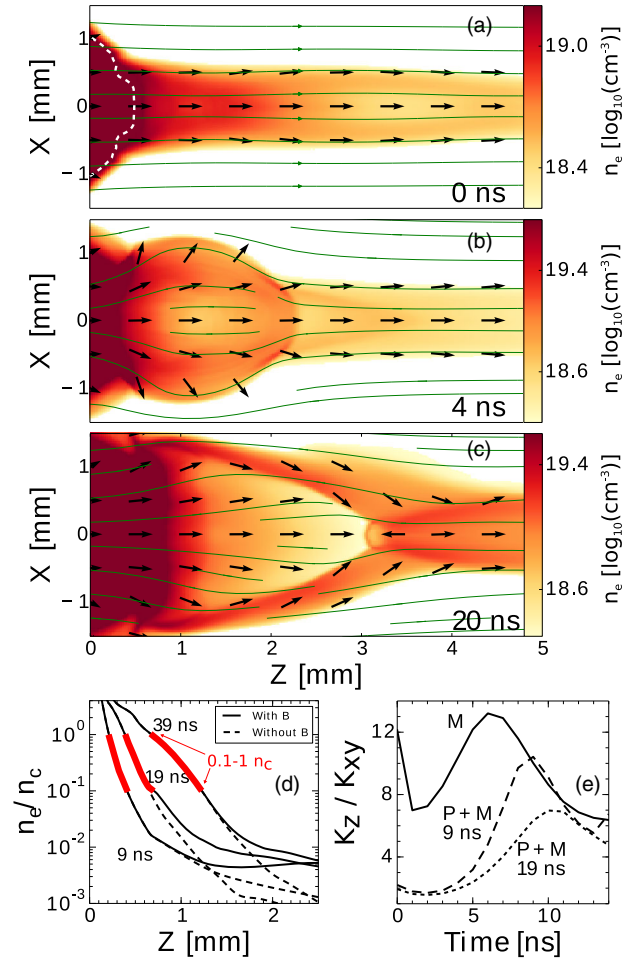


FIG. 5. 3D MHD simulations results. (a)–(c) Pseudocolor maps of  $n_e$  in the two-pulse configuration with a 19 ns delay. Times are measured from the main-pulse arrival. Arrows represent fluid velocity (not scaled in magnitude) and magnetic field lines are shown. Panel (a) shows the plasma created by the low energy precursor at a time just before the arrival of the main pulse. The white dashed line corresponds to the isocontour at  $0.1n_c$ . (d) Profiles of  $n_e$ , averaged over the laser focal spot, for a case of precursor-only irradiation at 9, 19, and 39 ns after precursor irradiation. Cases with (solid line) and without (dashed line) magnetic field are shown. (e) Ratio of longitudinal ( $K_z = 0.5\rho v_z^2$ ) to radial [ $K_{xy} = 0.5\rho(v_x^2 + v_y^2)$ ] kinetic energy integrated over the entire plasma volume, for the main-pulse-only (M) and the temporally staged cases (P + M).

around  $10^\circ$  with main pulse only to  $50^\circ$  for two pulses with 19 ns delay [see Figs. 2(d)–2(f)]. This variation is consistent with the cavity shape becoming more spherical: the flow converges at the tip of the cavity almost head-on. The more planarlike collision leads to an increased thermalization of the flow’s kinetic energy, higher temperatures, and thus more diverging flows. A similar effect is discussed in the astrophysical literature in the context of jet formation by the convergence of supersonic conical flows [31]. Remarkably, the experiments show that the recollimating conical shock is quasisteady state and independent of

the presence of an ambient plasma or of the laser irradiation delay, and that the collimation is very effective even for more isotropically expanding ejections. These results strengthen the claim made in Refs. [14,15] that the recollimating conical shock may be at the origin of the stationary x-ray emission detected in some jets from young stellar objects [32–34].

Past the conical shock, the jet properties are also modified. In addition to an increase in temperature, the simulations show that the two-pulse configuration increases the jet’s mass flux ( $\rho v_z$ ) and kinetic energy flux ( $\rho v^2 v_z/2$ ) by  $\sim 10$ , and create velocity variations,  $\Delta v_z \sim 100$  km/s (Mach 2–3), which drive shocks within the jet itself. This is consistent with observations of astrophysical jets that indicate it is the unsteadiness of mass ejection that drives shocks (so called “knots”) inside the jet body (see Ref. [21] for a review). The results presented here thus provide a first glimpse of the effects of time variability on the formation and stability of the recollimation shock and on the jet itself.

In summary, we have presented a study of the interaction of two, temporally staged, high-power laser pulses with a solid target in the presence of a 20 T magnetic field aligned along the main axis of the plasma expansion. The precursor laser pulse generates a plasma that is collimated by the magnetic field into a jet. The ensuing plasma dynamics can then be controlled by delaying the arrival of the second (main) pulse, so that its absorption occurs further away from the initial target and over larger volumes. However, even at this relatively high field strength, we see no impact of the magnetic field on the laser absorption itself, a finding that may be of particular interest to the (magnetized) inertial confinement fusion community. The time delay between the two laser pulses has clear effects on the plasma: a more divergent cavity expansion, higher electron temperatures, and stronger shocks; yet, long-lived, stable astrophysically relevant jets are still formed. This control over the flow dynamics and variability opens the door to a range of new laboratory studies related to variable accretion [13] and ejection phenomena in astrophysics.

The authors acknowledge the support of the LULI technical teams in the execution of this work. We thank the Dresden High Magnetic Field Laboratory at Helmholtz-Zentrum Dresden-Rossendorf for the development of the pulsed power generator, and B. Albertazzi and M. Nakatsutsumi for prior work in developing the experimental platform. This work was supported by grants from Région Ile-de-France (DIM ACAV). This work was supported by ANR Blanc Grant No. 12-BS09-025-01 SILAMPA and was partly done within the LABEX Plas@Par project supported by Grant No. 11-IDEX-0004-02 from Agence Nationale de la Recherche and by the LABEX CALSIMLAB. This work was supported in part by the Ministry of Education and Science of the Russian Federation under Contract No. 14.Z50.31.0007 and Competitiveness Program of NRNU MEPhI. X-ray

spectroscopy data measurements and analysis were made by JIHT RAS group under financial support of the Russian Science Foundation (Grant No. 14-50-00124). O. W. acknowledges the DFG Programmes GRK 1203 and SFB/TR18. This work was performed under the auspices of the U.S. Department of Energy by Lawrence Livermore National Laboratory under Contract No. DE-AC52-07NA27344. A. S. acknowledges the support of RFBR foundation in the frame of Projects No. 16-32-60183. M. B. and K. N. acknowledge funding from EPSRC (Grants No. EP/J500094/1 and No. EP/I029206/1).

---

\*higginson2@llnl.gov

- [1] D. R. Farley, K. G. Estabrook, S. G. Glendinning, S. H. Glenzer, B. A. Remington, K. Shigemori, J. M. Stone, R. J. Wallace, G. B. Zimmerman, and J. A. Harte, *Phys. Rev. Lett.* **83**, 1982 (1999).
- [2] R. Yurchak, A. Ravasio, A. Pelka, S. Pikuz, Jr, E. Falize, T. Vinci, M. Koenig, B. Loupias, A. Benuzzi-Mounaix, M. Fatenejad *et al.*, *Phys. Rev. Lett.* **112**, 155001 (2014).
- [3] A. Kasperczuk, T. Pisarczyk, S. Borodziuk, J. Ullschmied, E. Krousky, K. Masek, K. Rohlena, J. Skala, and H. Hora, *Phys. Plasmas* **13**, 062704 (2006).
- [4] P. Nicolai, V. T. Tikhonchuk, A. Kasperczuk, T. Pisarczyk, S. Borodziuk, K. Rohlena, and J. Ullschmied, *Phys. Plasmas* **13**, 062701 (2006).
- [5] L. J. Perkins, B. G. Logan, G. B. Zimmerman, and C. J. Werner, *Phys. Plasmas* **20**, 072708 (2013).
- [6] S. A. Slutz, M. C. Herrmann, R. A. Vesey, A. B. Sefkow, D. B. Sinars, D. C. Rovang, K. J. Peterson, and M. E. Cuneo, *Phys. Plasmas* **17**, 056303 (2010); S. A. Slutz and R. A. Vesey, *Phys. Rev. Lett.* **108**, 025003 (2012).
- [7] B. Srinivasan and X.-Z. Tang, *Phys. Plasmas* **20**, 056307 (2013).
- [8] T. Sano, T. Inoue, and K. Nishihara, *Phys. Rev. Lett.* **111**, 205001 (2013).
- [9] P. Y. Chang, G. Fiksel, M. Hohenberger, J. P. Knauer, R. Betti, F. J. Marshall, D. D. Meyerhofer, F. H. Séguin, and R. D. Trasso, *Phys. Rev. Lett.* **107**, 035006 (2011).
- [10] D. H. Froula, J. S. Ross, B. B. Pollock, P. Davis, A. N. James, L. Divol, M. J. Edwards, A. A. Offenberger, D. Price, R. P. J. Town *et al.*, *Phys. Rev. Lett.* **98**, 135001 (2007).
- [11] D. S. Montgomery *et al.*, *Phys. Plasmas* **22**, 010703 (2015).
- [12] D. B. Schaeffer, W. Fox, D. Haberberger, G. Fiksel, A. Bhattacharjee, D. H. Barnak, S. X. Hu, and K. Germaschewski, *Phys. Rev. Lett.* **119**, 025001 (2017).
- [13] G. Revet *et al.*, *Sci. Adv.* **3**, e1700982 (2017).
- [14] A. Ciardi, T. Vinci, J. Fuchs, B. Albertazzi, C. Riconda, H. Pépin, and O. Portugall, *Phys. Rev. Lett.* **110**, 025002 (2013).
- [15] B. Albertazzi *et al.*, *Science* **346**, 325 (2014).
- [16] M.-E. Manuel, C. Kuranz, A. Rasmus, S. Klein, M. MacDonald, M. Trantham, J. Fein, P. Belancourt, R. Young, P. Keiter *et al.*, *High Energy Density Phys.* **17**, 52 (2015).
- [17] D. Higginson, G. Revet, B. Khier, J. Béard, M. Blecher, M. Borghesi, K. Burdonov, S. Chen, E. Filippov, D. Khaghani *et al.*, *High Energy Density Phys.* **23**, 48 (2017).

- [18] B. Reipurth and J. Bally, *Annu. Rev. Astron. Astrophys.* **39**, 403 (2001).
- [19] A. Ferrari, *Annu. Rev. Astron. Astrophys.* **36**, 539 (1998).
- [20] R. E. Pudritz, M. J. Hardcastle, and D. C. Gabuzda, *Space Sci. Rev.* **169**, 27 (2012).
- [21] A. Frank, T. Ray, S. Cabrit, P. Hartigan, H. Arce, F. Bacciotti, J. Bally, M. Benisty, J. Eisloffel, M. Güdel *et al.*, *Protostars and Planets VI* (University of Arizona Press, Tucson, 2014), p. 451.
- [22] Y. Kato, K. Mima, N. Miyanaga, S. Arinaga, Y. Kitagawa, M. Nakatsuka, and C. Yamanaka, *Phys. Rev. Lett.* **53**, 1057 (1984).
- [23] B. Albertazzi *et al.*, *Rev. Sci. Instrum.* **84**, 043505 (2013).
- [24] S. N. Ryazantsev, I. Yu. Skobelev, A. Ya. Faenov, T. A. Pikuz, A. N. Grum-Grzhimailo, and S. A. Pikuz, *JETP Lett.* **102**, 707 (2015).
- [25] S. Ryazantsev, I. Y. Skobelev, A. Y. Faenov, T. Pikuz, D. Higginson, S. Chen, G. Revet, J. Béard, O. Portugall, A. Soloviev *et al.*, *Phys. Plasmas* **23**, 123301 (2016).
- [26] J. P. Chittenden, S. V. Lebedev, C. A. Jennings, S. N. Bland, and A. Ciardi, *Plasma Phys. Controlled Fusion* **46**, B457 (2004).
- [27] A. Ciardi, S. V. Lebedev, A. Frank, E. G. Blackman, J. P. Chittenden, C. J. Jennings, D. J. Ampleford, S. N. Bland, S. C. Bott, J. Rapley *et al.*, *Phys. Plasmas* **14**, 056501 (2007).
- [28] S. Atzeni, A. Schiavi, F. Califano, F. Cattani, F. Cornolti, D. D. Sarto, T. Liseykina, A. Macchi, and F. Pegoraro, *Comput. Phys. Commun.* **169**, 153 (2005).
- [29] K. Bockasten, *J. Opt. Soc. Am.* **51**, 943 (1961).
- [30] T. Vinci and A. Flacco, <https://github.com/aflux/neutrino>.
- [31] J. Canto, G. Tenorio-Tagle, and M. Rozyczka, *Astron. Astrophys.* **192**, 287 (1988).
- [32] F. Favata, C. V. M. Fridlund, G. Micela, S. Sciortino, and A. A. Kaas, *Astron. Astrophys.* **386**, 204 (2002).
- [33] J. Bally, E. Feigelson, and B. Reipurth, *Astrophys. J.* **584**, 843 (2003).
- [34] S. Ustamujic, S. Orlando, R. Bonito, M. Miceli, A. G. de Castro, and J. López-Santiago, *Astron. Astrophys.* **596**, A99 (2016).